JOURNAL OF THERMOPHYSICS AND HEAT TRANSFER
Vol. 25, No. 3, July–September 2011

Investigation of Martian-Dust Drag and Heat Transfer for Mars Sample Return Mission

T. Ozawa,* T. Suzuki,† H. Takayanagki,† and K. Fujita‡
Japan Aerospace Exploration Agency, Tokyo 182-8522, Japan

DOI: 10.2514/1.50714

A Mars nonstop dust sample return project has been proposed in a Mars exploration mission at Japan Aerospace Exploration Agency. To improve the feasibility of this project, the effect of a hot-temperature shock to dust particles was estimated by simulating particle motion, heat transfer, and thermal decomposition. When dust particles travel through the hot-temperature shock, which was calculated by the computational fluid dynamics and direct simulation Monte Carlo, three heat transfer models were compared for the estimation of Martian-dust heating. The results obtained from the macroscopic models were compared with microscopic direct simulation Monte Carlo calculations, and direct simulation Monte Carlo results were found to agree better with the Koshmarov and Svirshevskii and free-molecule models than the Kavanau model. In accordance with the investigation of heat transfer and thermal decomposition of dust particles, it was found that dust-particle sampling is feasible despite the heating due to the interaction with the shock, and the dust constituents are able to survive during the sampling.

Nomenclature

a	=	parameters used in Eqs. (28) and (29)
c	=	specific heat capacity, J/kg-K
C_D	=	drag coefficient
C_h	=	normalized heat transfer coefficient
C_{LR}	=	magnus lift-force coefficient
D	=	mass diffusivity, m^2/s
d	=	diameter, m
F_D	=	drag force, N
$\mathbf{F}_g$	=	gas force exerted on a particle
$\mathbf{F}_{LG}$	=	lift force due to velocity gradient
F_{num}	=	number of real molecules represented by a single DSMC molecule
f_r	=	recovery factor
f_{Tad}	=	ratio of adiabatic to gas temperature, T_{ad}/T_g
H	=	scaling height, km
h	=	heat transfer coefficient, W/m^2-K
j	=	translational and rotational degree of freedom
j_v	=	vibrational degree of freedom
Kn	=	Knudsen number
K_f	=	forward chemical reaction coefficient
k_m	=	mean mass transfer coefficient, kg/s-m^2
l_s	=	shock standoff distance, m
M	=	Mach number
M_{mol}	=	molar mass, g/mol
m	=	mass, kg
Nu	=	Nusselt number
N_A	=	Avogadro constant, mol^{-1}
N_{col}	=	number of collisions per time step
n	=	number density, m^{-3}
Pr	=	Prandtl number
p	=	pressure, Pa
Q	=	transferred energy, J
q	=	transferred energy rate, W
R	=	gas constant, 8.31447 J/K-mol
Re	=	Reynolds number
r	=	radius, m
r_{eff}	=	weighted mean radius of cross section, μm
r_m	=	normalization radius parameter in Eq. (29)
S	=	speed ratio
Sc	=	Schmidt number
Sh	=	Sherwood number
T	=	temperature, K
T_e	=	electron temperature, K
T_{rot}	=	rotational temperature, K
T_{tr}	=	translational temperature, K
T_{vib}	=	vibrational temperature, K
$\mathbf{u}$	=	gas velocity, m/s
V_d	=	volume of a dust particle, m^{-3}
$\mathbf{v}$	=	particle velocity, m/s
v_{eff}	=	weighted mean variance of cross section, μm
$\mathbf{w}$	=	particle rotational velocity, m/s
z	=	altitude, km
α	=	accommodation coefficient
γ	=	specific heat ratio
θ_v	=	characteristic vibrational energy, K
λ	=	thermal conductivity, W/m-K
μ	=	coefficient of viscosity, Pa-s
ν	=	kinematic viscosity, m^2/s
ρ	=	density, kg/m^3
Ω	=	collision integral
ω	=	viscosity index

Subscripts

ad	=	adiabatic
c	=	cell
col	=	collision
D	=	drag
d	=	dust
FM	=	free molecule
g	=	gas
Kav	=	Kavanau
p	=	particle
R	=	relative
r	=	rotational

Presented as Paper 2010-886 at the 48th AIAA Aerospace Sciences Meeting, Orlando, FL, 4–7 January 2010; received 11 May 2010; revision received 20 March 2011; accepted for publication 22 March 2011. Copyright © 2011 by the American Institute of Aeronautics and Astronautics, Inc. All rights reserved. Copies of this paper may be made for personal or internal use, on condition that the copier pay the $10.00 per-copy fee to the Copyright Clearance Center, Inc., 222 Rosewood Drive, Danvers, MA 01923; include the code 0887-8722/11 and $10.00 in correspondence with the CCC.

*Researcher, Aerospace Research and Development Directorate; 7-44-1 Jindaiji Higashi, Chofu; ozawa.takashi@jaxa.jp. Member AIAA.

†Researcher, Aerospace Research and Development Directorate, 7-44-1 Jindaiji Higashi, Chofu. Member AIAA.

‡Chief Researcher, Aerospace Research and Development Directorate, 7-44-1 Jindaiji Higashi, Chofu; fujita.kazuhisa@jaxa.jp. Senior Member AIAA.

v = vibrational or vertical
vap = vapor
0 = stagnation

Superscripts

cont = continuum
post = postcollisional quantity
pre = precollisional quantity
* = normalized quantity

I. Introduction

MARS exploration systems have been in high demand from the view of aeronomical and meteorological researchers. The PLANET-B (Nozomi) [1] spacecraft, the first Mars exploration mission at Japan Aerospace Exploration Agency (JAXA), was launched in 1998 and approached Mars in 2003. However, the mission did not succeed in putting its probe into a Martian orbit. In May 2003, the Institute of Space and Astronautical Science (ISAS) of Japan launched the Mu Science Engineering Satellite (MUSES)-C [2–4] spacecraft toward Asteroid 1998SF36 Itokawa. After the launch, the spacecraft was renamed "Hayabusa," and it is coming back to the earth with the asteroid samples. To continue the success of Japanese aerospace exploration and science technology, the Mars Exploration with Lander-Orbiter Synergy (MELOS) mission has come under review in JAXA together with many planetary scientific groups all over Japan.

In the MELOS mission, the following projects have been proposed to challenge scientific objectives. Primarily, an orbiter project has been planned to understand the circulation and exchange of Martian atmosphere from meteorological perspectives. Second, a Martian airplane project has been planned to observe the Martian surface and provide information of the crustal magnetism structure and evolution of Martian atmosphere, surface, and interior, as well as the understanding of the aerodynamics in a dilute gas environment. In addition to the above, additional probe vehicles can be incorporated into the MELOS mission. As one of the candidates, a lander project has also been planned for noble-gas isotopic measurements to understand how Mars atmosphere has evolved. Furthermore, a nonstop Mars sample return project, named Mars Aeroflyby Sample Collection (MASC), has also been proposed in our group [5,6]. One of the objectives on this project is to sample microscale dust particles [7] and establish the chemical, isotopic, and mineralogical composition of Martian dust and determine the extent of aqueous processing of Martian crustal materials [8]. Another is to use aerocapture technologies in order to reduce the size of the exploration system and the amount of propellant for orbital maneuver and liftoff. It is considered that microscale dust particles are widespread in the Martian atmosphere up to the altitude of 35–45 km above the ground. Therefore, if the spacecraft is able to fly by at these low altitudes without touchdown, the mission feasibility is expected to be considerably increased. The investigation of the aerocapture technique and the interplanetary orbital maneuver for the Mars exploration has been performed by Fujita et al. [5], and the flight path was optimized. The spacecraft geometry was also investigated by Takayanagi et al. [9] to fulfill conditions of the ballistic coefficient, the ratio of lift to drag, and so forth. As seen in Fig. 1, the shape was determined to be a sphere cone with the sphere radius of 0.35 m, the cone angle of 20 deg and the base diameter of 1.5 m. Nonetheless, the possibility of capturing floating-Martian-dust particles in the CO_2-based atmosphere has not been well investigated before, and several unproven factors, such as the effect of a hot-temperature shock on micron-sized particles and aerogel, the impact of hypervelocity dust particles on aerogel, and the heat transfer between dust particles and aerogel, need to be clarified to improve the feasibility of the project. In particular, investigation into the survivability of a micron-sized dust particle and its properties as it travels through a hot-temperature shock is crucial for the success of the Mars sample return mission.

Recently, a Mars Scout mission concept, Sample Collection for Investigation of Mars (SCIM), has been studied [10]. SCIM seeks to return Martian-dust samples and atmosphere to Earth without landing. Jurewicz et al. [11] investigated the use of aerogel sample collectors for SCIM, and the erosion of aerogel and the dust-particle temperature were predicted. However, the influence of a hot-temperature shock on the micron-sized dust particles has not been well reported.

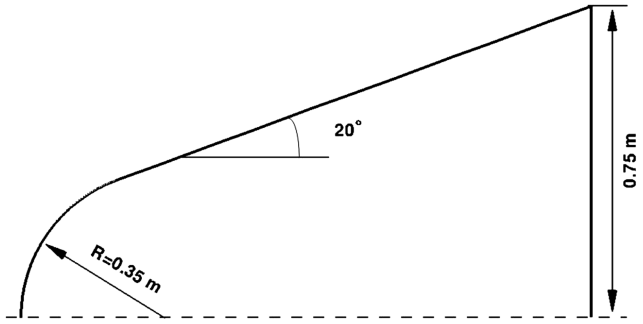

Fig. 1 Geometry of Mars entry vehicle.

For the Martian-dust flowfield, several effects, such as inertial [12], rarefaction, or compressibility, need to be considered for the drag and heat transfer models in high-temperature range. In the past, similar conditions have been studied in a solid fuel rocket nozzle field [13,14]. With the consideration of compressibility and rarefaction effects, the drag coefficient [13,15–17] was generally expressed as a function of Reynolds number and Mach number. Likewise, for the heat transfer equation, several models [18–20] have been developed to the low Reynolds number, rarefied flows from subsonic to supersonic region.

Nonetheless, there are several contributing factors that make the estimation of Martian-dust heating complicated. First, the flowfield is a CO_2-based gas mixture and varies from subsonic to supersonic in the rarefied, hot-temperature flow regime, where the transport coefficients are not well known. Second, a shock structure depends on the shape of spacecraft, ablators, and flight path. Third, the composition of the Martian dust is not known perfectly, whereas its composition was predicted to be a montmorillonite-basalt [21] or palagonitelike [22] composition by aeronomers and meteorologists in the past. Therefore, in this work, in order to improve the dust-particle heating estimation due to the shock, both macroscopic and microscopic computations have been performed. To begin with, particle simulations have been implemented using the macroparameters, such as drag coefficients and Nusselt numbers. Then the reliability of the macroscopic models has been investigated by comparing with the microscopic direct simulation Monte Carlo (DSMC) calculations.

This paper is organized as follows: The modeling of particle motion, heat transfer, and thermal decomposition is introduced in Secs. II, III, and IV. The numerical flow modeling technique in the computational fluid dynamics (CFD) and DSMC methods will be discussed in Sec. V. In Sec. VI, first, investigation of dust-particle distributions are shown, and second, the Martian-dust-particle trajectory and its heating and destruction inside a shock generated by the spacecraft for the nonstop sample return mission to Mars [23] are investigated. Conclusions are summarized in Sec. VII.

II. Modeling of Particle Motion

The equation of translational motion for a dust particle is

$$\frac{\mathrm{d}(m_d \mathbf{v})}{\mathrm{d}t} = -V_d \nabla p + \mathbf{F}_g \tag{1}$$

where m_d and V_d are the mass and volume of a dust particle, $\mathbf{v}$ is the particle velocity, and $\mathbf{F}_g$ is the gas force exerted on the particle. The term of gravitational acceleration is neglected in this work. The subscripts g and d denote the gas and dust particle, respectively. The gas force $\mathbf{F}_g$ can be given by [24,25]

$$\mathbf{F}_g = \frac{1}{2}\rho_g \pi r_d^2 |\mathbf{u}_R| \left(C_D \mathbf{u}_R + C_{LR} \frac{\mathbf{u}_R \times \mathbf{w}_R}{|\mathbf{w}_R|} \right) + \mathbf{F}_{LG} \tag{2}$$

The gas velocity relative to the particle is $\mathbf{u}_R = \mathbf{u} - \mathbf{v}$, where $\mathbf{u}$ is the gas flow velocity. $\mathbf{w}_R$ is the rotational velocity of the particle relative to the gas. C_D is the nondimensional drag coefficient. In Eq. (2), the second term, the Magnus lift force, and $\mathbf{F}_{LG}$, the lift force due to velocity gradient, are neglected in this work because the first term, the drag force, is dominant in our case. The equation of particle motion can be simplified as [26]

$$\frac{\mathrm{d}\mathbf{v}}{\mathrm{d}t} = -\frac{\nabla p}{\rho_d} + \frac{3}{8 r_d}\frac{\rho_g}{\rho_d} C_D |\mathbf{u}_R| \mathbf{u}_R \tag{3}$$

Note that $\rho_d \gg \rho_g$, and thus the particle trajectory, is barely influenced by the atmosphere in the shock. Although the Martian-dust particles may have platelike shapes, they are assumed to be a sphere shape in this work. This is considered to be a reasonable assumption for modeling the interaction of the dust particles with the flowfield because of the random orientation. Their size is also assumed to be between 1 and 10 μm. In our cases, several effects such as inertial [12], rarefaction, or compressibility need to be considered for the drag coefficient equation. In a solid fuel rocket nozzle field, the motion of small solid particles in the hot gases has been studied [13,15,16], and the drag coefficient was found to be a function of Reynolds number, $Re_d = 2r_d|\mathbf{u} - \mathbf{v}|/\nu_g$, and Mach number, where ν_g is the kinematic viscosity and is μ_g/ρ_g. Since the Reynolds number of the particle is basically lower than 1 in this work, the Stokes's law of resistance with an inertial correction can be written as [27]

$$C_{D,\mathrm{inc}} = \frac{24}{Re_d}(1 + 0.15 Re_d^{0.687}) \tag{4}$$

With compressibility and rarefaction effects, the drag coefficient equation is expressed as [17]

$$\begin{aligned} C_D &= \frac{F_D}{0.5\rho_g|\mathbf{u} - \mathbf{v}|^2 \pi r_d^2} \\ &= 2 + (C_{D,\mathrm{inc}} - 2)\exp\left[-\frac{3.07\sqrt{\gamma} M G(Re_d)}{Re_d} \right] \\ &\quad + \frac{H(M)\exp[-\frac{Re_d}{2M}]}{\sqrt{\gamma} M} \end{aligned} \tag{5}$$

which is based on the Crowe's equation [28] and is substituted by simpler functions. Two auxiliary functions, $G(Re_d)$ and $H(M)$ is given by

$$\begin{aligned} \log_{10} G(Re_d) &= \frac{2.5(Re_d/312)^{0.6688}}{1 + (Re_d/312)^{0.6688}} \\ H(M) &= \frac{4.6}{1 + M} + 1.7\sqrt{\frac{T_d}{T_g}} \end{aligned} \tag{6}$$

Assuming that the Mars entry flowfield will not be influenced by a particle (e.g., the mass loading ratio is approximately 10^{-4}), the flowfield will be calculated by the CFD [29,30] or the DSMC [31] method in advance, separately. From the flowfield calculation, the gas velocity, density, pressure, and so forth, in each cell can be obtained, and the influence of the flowfield on a dust particle will be calculated.

III. Modeling of Particle Heat Transfer

The heat transfer rate for a dust particle due to heat conduction is defined using the thermal conductivity and Nusselt number as

$$\frac{\mathrm{d}Q}{\mathrm{d}t} = Nu\lambda_g(T_{\mathrm{ad}} - T_d) \times 2\pi r_d \tag{7}$$

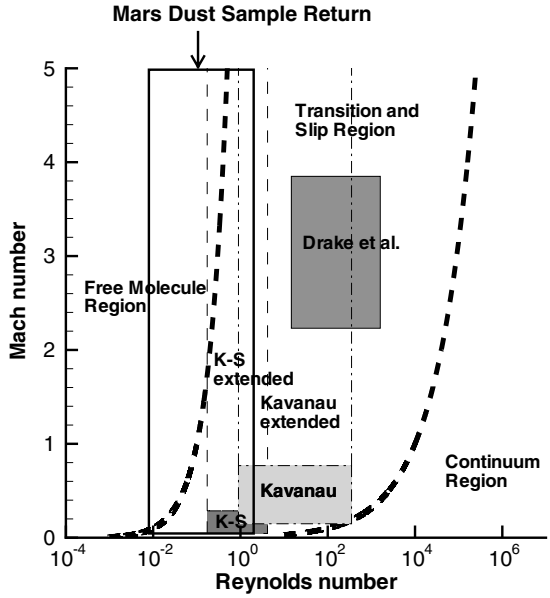

Fig. 2 Flow regions of gas dynamics and a flow region for the Mars-dust sample collection.

The flow region for the Mars-dust sample return are defined as functions of Mach and Reynolds numbers and are shown in Fig. 2. In the figure, regions for three models [18–20] that have been applied to the low Reynolds number, rarefied flows from subsonic to supersonic are also shown and compared with the flow region for the Mars-dust sample capture. It is shown that the Reynolds number for the region is approximately between 0.01 and 1.0, and the Mach number is from subsonic to supersonic, which overlaps with the modified Kavanau model [18] and Koshmarov and Svirshevskii (K-S) model [19]. The flow region in this work is similar to solid rocket plume environments, and Nelson and Fields [13,14] have investigated the Nusselt number model for the solid rocket plume conditions by comparing with the DSMC results. He found that the Kavanau [18] and the K-S [19] correlations yielded good predictions of the Nusselt number for high-temperature rarefied conditions. Since the dust-particle heating prediction strongly relies on the heat transfer coefficient or the Nusselt number, the modeling of heat transfer should be carefully investigated. In this work, we apply these two models to evaluate the Nusselt number in addition to the free-molecule (F-M) model, and then these models are compared with the microscopic DSMC results.

The adiabatic temperature T_{ad} in Eq. (7) is defined as

$$T_{\mathrm{ad}} = \left(1 + \frac{\gamma - 1}{2} M^2 f_r\right) T_g \tag{8}$$

where f_r is the recovery factor. If f_r is not mentioned specifically, $f_r = \sqrt{Pr_0}$ will be used [19]. To begin with, CO_2 properties are used as the gas properties in this work, since the 95% of the Mars atmosphere is CO_2. Both the viscosity coefficient μ_g and the thermal conductivity λ_g were calculated by the cubic spline interpolation or extrapolation using the data of Vesovic and Wakeham [32].

The temperature change of a particle due to the heat transfer is simply calculated as

$$\Delta T_d = \Delta Q/(\rho_d V_d c_d) \tag{9}$$

because the particle size considered in this work is so small that the particle temperature can be assumed to be uniform. Note that the Biot number in the flowfield is smaller than 0.3 even for $r_d = 10$ μm. For the specific heat capacity of the dust particle, since the main constituent of the Martian dust is silica, data for silica [33,34] was used in this work.

A. Modified Kavanau Model

Among the three models, the Kavanau model [18] was first selected for the heat transfer calculations because of its simplicity and fair accuracy in the flow regime where we are interested. This model was originally developed in the subsonic region, and the Mach number correction was used to extend this model to the rarefied gas limit and high Mach number [17]. The Nusselt number Nu is written as [35]

$$Nu_{\text{Kav}} = \frac{Nu^{\text{cont}}}{1 + 3.42(M'/Re_d Pr_g)Nu^{\text{cont}}} \tag{10}$$

where Nu^{cont} is the continuum limit of the Nusselt number, and Pr_g is the Prandtl number, $Pr_g = c_g\mu_g/\lambda_g$. Nu^{cont} is calculated as

$$Nu^{\text{cont}} = 2 + 0.459 \times Pr_g^{0.33} Re_d^{0.55} \tag{11}$$

M' is the corrected Mach number, and

$$M' = \frac{M}{1 + 0.428M(1 + 1/\gamma)} \tag{12}$$

B. Free-Molecule Model

The F-M model [36] was originally developed to predict convective heat transfer and recovery factors for low-temperature flows. In this work, the F-M model with the consideration of vibrational excitation effects was used to calculate heat transfer in the high-temperature conditions. In the F-M model, the nondimensional convective heat flux, q^* is calculated as [37]

$$q^*_{\text{FM}} = -\left[\left(2 + \frac{j_r}{2} + \frac{j_{vd}}{2}\right)(G^* + F^*)\frac{T_d}{T_g} - \left(S^2 + \frac{5 + j_r}{2} + \frac{j_{vg}}{2}\right)\left(G^* + F^* + \frac{G^*}{2}\right)\right] \tag{13}$$

where S is the speed ratio ($S = \sqrt{\gamma/2}M$), for a sphere shape,

$$G^* = \frac{\text{erf}(S)}{4S^2}, \qquad F^* = \frac{1}{4}\left[\frac{\exp(-S^2)}{\sqrt{\pi}S} + \frac{2S^2 - 1}{2S^2}\text{erf}(S)\right] \tag{14}$$

j_r is 2 for CO_2, and j_v is the vibrational degree of freedom, which can be calculated as

$$j_v = \sum_{i=1}^{I} \frac{2\theta_{v,i}/T}{\exp(\theta_{v,i}/T) - 1} \tag{15}$$

Since CO_2 has four vibrational modes, I is equal to 4 in this work. The heat transfer rate depends on the accommodation coefficient α and is expressed as

$$q_{\text{FM}} = \pi d_d^2 \alpha p_g v_R q^*_{\text{FM}} \tag{16}$$

and the heat transfer coefficient, h_{FM}, is

$$h_{\text{FM}} = q_{\text{FM}}/[\pi d_d^2(T_{\text{ad}} - T_d)] \tag{17}$$

The Nusselt number is calculated as

$$Nu_{\text{FM}} = h_{\text{FM}} d_d/\lambda_g \tag{18}$$

The adiabatic temperature in this model is calculated by solving for T_d such that $T_d = T_{\text{ad}}$ when q^*_{FM} is equal to 0 in Eq. (13).

C. Koshmarov and Svirshevskii Model

The K-S [19] model is also employed in this work. This model is a developed empirical correlation equation for spheres at Mach numbers from subsonic to supersonic in slip and rarefied flows.

The Nusselt number is obtained from

$$Nu_{\text{KS}} = [H(h_{\text{FM}} + h_{\text{KS}}) - h_{\text{KS}}]d_d/\lambda_g \tag{19}$$

where h_{KS} and H are the K-S correlation heat transfer coefficient and a factor obtained from experimental dependence, respectively, and they can be found in [19].

IV. Modeling of Particle Decomposition

Thermal decomposition can also be an important process when dust particles are heated by a hot-temperature shock. The process is modeled as mass transfer from the particle to the atmosphere. The mass transfer rate [38] is calculated as

$$\frac{\text{d}m_d}{\text{d}t} = -k_m 4\pi r_d^2 \frac{x_d}{1 - x_d} \tag{20}$$

where k_m is the mean mass transfer coefficient in units of kg/s-m^2, x_d is the mole fraction of the dust particle, and k_m is calculated as [38]

$$k_m = \frac{\rho_g D_{dg}}{2r_d} Sh \tag{21}$$

where D_{dg} is the mass diffusivity, and Sh is the Sherwood number. The mass diffusivity is calculated from the Chapman–Enskog kinetic theory as

$$D_{dg} = \frac{3}{16}\sqrt{\frac{2 \times 10^3 (RT_g)^3}{\pi}\left(\frac{1}{M_{\text{mol},d}} + \frac{1}{M_{\text{mol},g}}\right)}\frac{1}{N_A p d^2 \Omega_D} \tag{22}$$

The Sherwood number is obtained from

$$Sh = 2 + 0.6Sc^{1/3}Re^{1/2} \tag{23}$$

where Sc is the Schmidt number ($Sc = \nu_g/D_{dg}$). The mole fraction of the particle, x_d is calculated from the vapor pressure [39] as

$$x_d = \frac{p_{\text{vap}}(T_d)}{p_g} \tag{24}$$

The decrease of the particle mass also changes the size of the particle.

The main composition of the Martian-dust particles is considered to be either montmorillonitelike [21] or palagonitelike [22], and montmorillonite and palagonite are composed of 63 and 31% of SiO_2, respectively. Thus, in this work the dust-particle properties are represented by the well-known SiO_2. The mole fraction of the particle is obtained from the vapor pressure [39], which is a function of temperature, and the other properties of a dust particle as the initial condition are listed in Table 1.

V. Modeling of Mars Entry Flowfield Calculations

To investigate the influence of a hot-temperature shock on the micron-sized dust particles, Mars atmosphere entry flowfields and the shock structures need to be obtained at descent altitudes for the dust sampling, and thus in this work, 2-D axisymmetric CFD and DSMC computations have been performed for Mars entry flowfields at 35 and 45 km altitudes. Freestream conditions, such as the total number density, temperature, speed, and mole fractions of chemical species, at 35 and 45 km altitudes for the Mars entry are listed in Table 2. As shown in the table, the number density at 45 km is considerably lower than the 35 km case, and the continuum assumption may not be applicable for the hypersonic bow-shock flows at this altitude due to the breakdown effect. Therefore, the DSMC particle simulations have been carried out for the 45 km case instead of the continuum method while 2-D axisymmetric CFD

Table 1 Dust-particle properties

Parameter	Initial value
Molar mass, g/mol	60.08
Temperature, K	T_∞
Speed, m/s	v_∞
Radius, μm	1, 2, or 10

Table 2 Mars entry conditions

Altitude	35 km	45 km
Number density, m^{-3}	5.8452×10^{21}	1.6×10^{21}
Temperature, K	171	152.67
Speed, km/s	4.194	5.0
CO_2	0.967	0.971
N2	0.027	0.027
Ar	0.016	0.0
O_2	0.0	0.0017
CO	0.0	0.0007

calculations have been performed at 35 km. For the CFD computations, the JAXA Optimized Nonequilibrium Aerothermodynamic Analysis (JONATHAN) code [40] has been used in this work. For the DSMC computations, a new DSMC code, named Modeling Of Transitional-Ionized Flows (MOTIF), has been developed at JAXA recently.

In CFD, 17 species (N, O, C, N_2, O_2, NO, C_2, CN, CO, C_3, CO_2, C^+, O^+, O_2^+, CO^+, NO_+, and e^-) were considered in the flow, and a two-temperature model was used [30]. Thermochemical models used for reacting CO_2 flows are summarized in [41–44]. In total, 33 types of chemical reactions including 11 types of dissociation reactions were considered in the calculations. Note that although ionization reactions and charged species were included in the thermochemical database, it was found that they are not important for our Mars entry conditions. The forward rate coefficient is calculated by an equation of the modified Arrhenius rate $K_f(T) = AT^B \exp(-E_a/k_BT)$, and the parameters are given in [30]. The backward rate coefficient is determined from K_f and the equilibrium constant, which is obtained from individual partition functions of chemical components involved in the reaction. The partition functions are calculated by the SPRADIAN2 [45] radiation code, which is linked with the CFD code for radiation coupled flowfield calculations. The Landau–Teller type relaxation model is used for vibrational relaxation with the parameters recommended in [42]. Also, a high-temperature correction is introduced using an imaginary cross section [42]. The coefficients of viscosity, thermal conductivity, and ordinary diffusion in a gas mixture are computed by the first-order expressions of Chapman–Enskog theory with modifications to take into account in the ambipolar electric field. The collision integrals are mostly taken from [43,46,47]. The convective numerical flux is formulated by the AUSM-DV scheme [48] with the second-order upwind-biased MUSCL scheme [49]. To settle the strong stiffness originating from chemical reactions, the diagonal implicit scheme [50] is applied to the chemical source terms, whereas the convective and the viscous terms are integrated explicitly in time using local time steps.

In DSMC, 8 species (N, O, C, N_2, O_2, NO, CO, and CO_2) were considered in the flow. The computational time step was chosen with the one associated with molecular collisions. In the code, the no-time-counter scheme [31] is employed for modeling the molecular collision frequency, and the variable-hard-sphere [51] model is used for modeling the collision cross section between particles. The variable-hard-sphere parameters can be found in [31]. The Borgnakke-Larsen [52] model with temperature-dependent rotational and vibrational relaxation numbers is used for modeling rotation-translation (R-T) and vibration-translation (V-T) energy transfers between neutral species. The Millikan and White [53] form of the relaxation time are used for V-T rates, and Parker's rates [54] are used for the R-T rates. For the DSMC calculation, the total collision energy (TCE) [31] model is used for modeling chemical reactions. In the TCE model, the reaction probability has a special form that allows one to match experimental reaction rates $K_f(T)$ in a modified Arrhenius form. A total of 54 chemical reactions including 40 dissociation reactions were considered in the calculation [55]. Note that reaction probabilities using the TCE model are lower than unity for the speed range studied in this work. The gas-surface interaction was modeled using the Maxwell model with total energy and momentum accommodation with a surface temperature of 500 K, and a noncatalytic wall condition was used. The time step, cell size, computational domain, and total number of simulated molecules were investigated to obtain results that are independent of these DSMC numerical parameters. At 45 km, approximately 2 million particles were simulated in the computational domain. The total numbers of collisions per time step and macroparameter cells were 768,000 and 192,000, respectively. The total number of time steps was about 40,000 with a time step of 4.0×10^{-8} s for 45 km altitude. Macroparameter sampling was started after a time step that was sufficient to reach the steady state (i.e., the number of particles and collisions becomes steady), which was 30,000 time steps for the 45 km case.

To investigate the drag and heat transfer coefficients in the flow regime specified in Fig. 2, the results obtained by the macroscopic models are compared with microscopic DSMC results. In DSMC, the drag force is calculated from the summation of particle momentum transfer as

$$F_D = \sum_p [(mv_{x,p}^{\text{pre}} - mv_{x,p}^{\text{post}}) F_{\text{num},p}] \Big/ \Delta t \tag{25}$$

where the freestream direction is set to the x direction, and the heat transfer rate is calculated from the summation of particle energy transfer as

$$q = \sum_p [(E_{\text{col},p}^{\text{pre}} - E_{\text{col},p}^{\text{post}}) F_{\text{num},p}] \Big/ \Delta t \tag{26}$$

The particle information is accumulated over the sampling time steps and the F_D and q are the average value over the sampling time to reduce the statistical noise. The nondimensional drag and heat transfer coefficients are calculated as follows:

$$C_D = \frac{F_D}{(\rho_\infty U_\infty^2/2) \times \pi r_d^2}, \qquad C_h = \frac{q}{(\rho_\infty U_\infty^3/2) \times \pi d_d^2} \tag{27}$$

The overall C_D and C_h are calculated in DSMC and compared with the macroscopic models.

VI. Results and Discussion

A. Dust-Particle Distributions

To optimize the aerogel size and the capturing time for the MASC project, Martian-dust vertical and size distributions at specific altitudes need to be investigated. In the past, a variety of particle size distributions have been proposed and discussed [56–58] on the several missions, such as Mariner 9 [21,22,59], Viking [57,60,61], Phobos [62,63], Mars Pathfinder [64,65], and so forth.

In this work, the vertical distribution of dust particles, n_v, is expressed as [59]

$$n_v(z) = \rho(z) a_0 \exp\{v_d[1 - \exp(z/H)]\} \tag{28}$$

where ρ is the atmosphere density in units of kg/m^3 obtained from Mars-GRAM database [66], and z is the altitude in a unit of km. The column number density was estimated to be 4.6×10^{10} m^{-2} in a dust-storm condition, and the parameter a_0, which is the specific concentration of the dust at $z = 0$, was calculated from the integration of $n_v(z)$. In an average condition, the column number density was estimated to be 4.75×10^9 m^{-2} in order to fit with $n_v(0) = 6 \times 10^5$ m^{-3}. Parameters used in Eq. (28) for the average and dust-storm cases are listed in Table 3. Figure 3 shows the dust-particle

Table 3 Parameters for the vertical distribution

Parameter	Average	Storm
v_d	0.1	0.007
H, km	10	10
a_0, g^{-1}	3.95×10^4	3.14×10^5

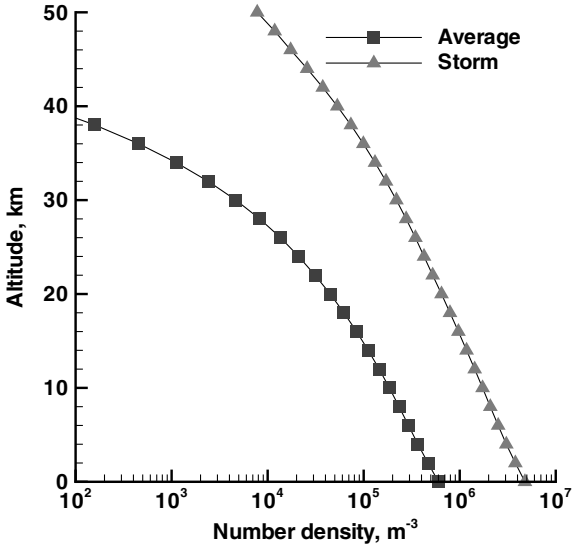

Fig. 3 Dust-particle vertical distribution between the average and the storm cases.

vertical distribution between the average and storm cases, and the significant difference can be seen between the two cases.

The modified gamma distributions were used to represent the dust-particle size distributions as [21,22]

$$\frac{\mathrm{d}n(r)}{\mathrm{d}r} = n_1 r^{a_1} \exp\left[-\frac{a_1}{a_2}\left(\frac{r}{r_m}\right)\right] \tag{29}$$

and Tomasko et al. [65], Markiewicz et al. [64], and Korablev et al. [62] used the simplified equation setting $a_2 = 1$ as

$$\frac{\mathrm{d}n(r)}{\mathrm{d}r} = n_1 r^{(1-3b)/b} \exp\left[-\frac{r}{r_{\mathrm{eff}} b}\right] \tag{30}$$

where r and r_{eff} is the particle radius and the effective radius, respectively. From Fig. 3, the dust-particle number density is set to 8×10^2 m^{-3} for the average case and 1×10^5 m^{-3} for the storm case at 35 km altitude, and a parameter n_1 was calculated from the integration of the size distribution over the dust radius. Korablev et al. [62] investigated the Martian atmosphere from the Phobos spacecraft in the altitude range of 12–35 km. They found that the dust number density at 30 km is approximately 3×10^4 m^{-3}, and the extrapolated value at 35 km is close to 1×10^3 m^{-3}. Since the Phobos observation was in a clear condition, this value is similar to our estimation for the average case ($n = 8 \times 10^2$ m^{-3}).

Five models are compared at 35 km, and the parameters used in the models are listed in Table 4. The effective radius is also listed in the table, and it is between 1 and 3 μm for all of the models. The dust-particle size distributions at 35 km altitude for the average (top) and storm (bottom) cases are presented in Fig. 4. As shown in the figure, the distributions are similar except for Clancy et al. [22], and the distribution of Toon et al. [21] predicts the highest density for the dust radius greater than 5 μm. Among the five models, the Toon et al. model shows the most broad distribution because the Mariner 9 observation was taken during the decay phase of a dust storm. Between the average and dust-storm cases, the number density is more than 1 order of magnitude higher for the storm case. The

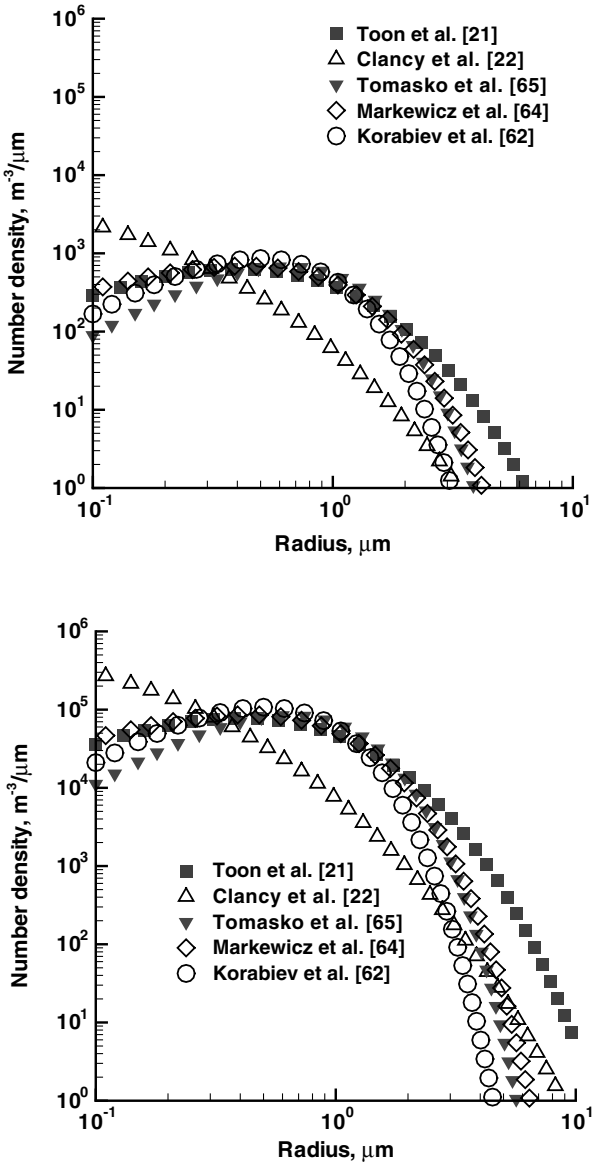

Fig. 4 Dust-particle size distribution at 35 km altitude for the average (top) and storm (bottom) cases.

distribution of Clancy et al. [22] predicts low number density for larger dust size, but other distributions predict the high dust number density similar to each other for the dust size range between 0.5 and 5 μm. Considering the aerogel surface area of 100 cm^2 and capturing samples at 35 km, dust particles between 0.5 and 5 μm that reach the aerogel is approximately 1.6×10^3/s for the average condition. For the storm condition, it is about 1.6×10^5/s. Therefore, there are a plenty of micron-sized dust samples to be captured at 35 km. At 45 km, the flux of dust particles to the aerogel is approximately 3/s for the average condition and 3×10^4 for the storm condition, and this indicates that if the Martian weather is in a clear condition, the sampling time needs to be longer than 1 s at 45 km or the sampling altitude needs to be lower than 45 km.

Table 4 Parameters for the particle size distribution

Model	Observation	Parameters	r_{eff}, μm
Toon et al. [21]	Mariner-9	$a_1 = 2$, $a_2 = 0.5$, $r_m = 0.4$	2.75
Clancy et al. [22]	Mariner-9 and Viking orbiter	$a_1 = 1$, $a_2 = 0.3$, $r_m = 0.014$	1.8
Tomasko et al. [65]	Mars Pathfinder	$b = 0.2$	1.6
Markiewicz et al. [64]	Mars Pathfinder	$b = 0.25$	1.71
Korablev et al. [62]	Phobos	$b = 0.2$	1.26

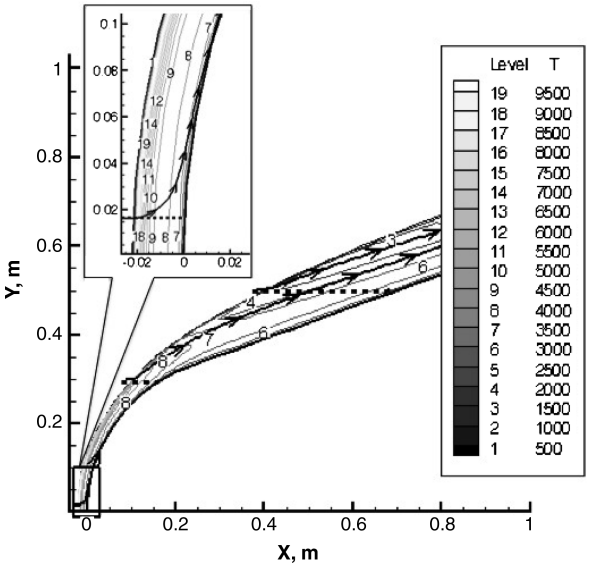

Fig. 5 A contour plot of translational temperature for the Mars atmosphere entry at 35 km and streamlines (solid line) and particle trajectories (dashed line).

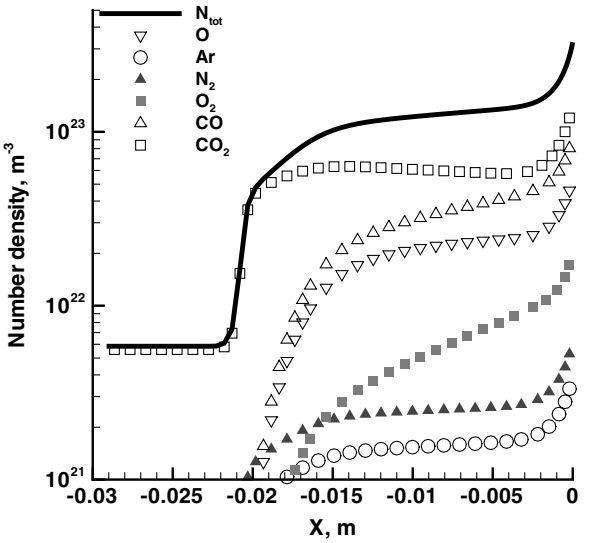

Fig. 7 Distributions of species number densities for the Mars atmosphere entry at 35 km along the stagnation line.

B. Mars Flowfield at 35 Kilometers

The target descent altitude for the sample capture is planned to be between 30 and 45 km for the MASC project [5] in JAXA. Thus, we investigate the Martian atmospheric gas- and dust-particle interactions at 35 km in this and the following two subsections, and the investigation at 45 km will be shown in subsections VI.E–VI.G. First, 2-D axisymmetric CFD calculations have been carried out for the Mars atmosphere entry flowfield at 35 km altitude. The freestream condition at this altitude for the Mars entry is listed in Table 2. In Fig. 5, a contour plot of translational temperature for the Mars atmosphere entry at 35 km is shown. In addition, streamlines (solid line) and 1 μm-dust-particle trajectories (dashed line) are compared from three initial different locations in the figure. The initial r coordinates of a dust particle are 0.0165, 0.3, and 0.5 m for trajectories 1–3, respectively. It can be seen that the trajectories of a dust particle are negligibly influenced by the shock, due to their heavy mass and do not follow the gas flow streamlines.

Mars entry flowfields along the stagnation line at 35 km obtained by the CFD calculations are shown in Figs. 6 and 7. It is shown that the shock standoff distance l_s is approximately 0.02 m. The temperature overshoot phenomenon can be seen, where the maximum temperature is approximately 10,000 K. In this region, the vibrational temperature is obviously lower than the translational temperature. However, in the postshock region, the difference between the translational and vibrational temperatures is negligibly small, and these temperatures are between 4000 and 5000 K. Note that in CFD the vehicle wall temperature was set to 1600 K, and a catalytic wall condition for charged species was used. The dissociation rate of CO_2 is so high that the rapid increase of the number densities of CO and O can be seen near the body. It was also found that the number densities of charged species are negligibly small in the flowfield, and thus they are not shown in Fig. 7.

C. Dust Heat Transfer at 35 Kilometers

Particle motion, heat transfer, and thermal decomposition of a micron-sized Martian-dust particle were simulated in the Mars entry flowfield at 35 km. The heating of dust particles in the stagnation region is presented in Fig. 8 as a function of time at 35 km. The accommodation coefficient of the dust-particle surface is set to unity for the calculations in Fig. 8. 1-, 2-, and 10-μm-sized dust particles are compared in the figure. Inside the shock, the particle temperature gradually increases, and the increase rate is higher for the smaller particle. It is noteworthy that from the sample return project

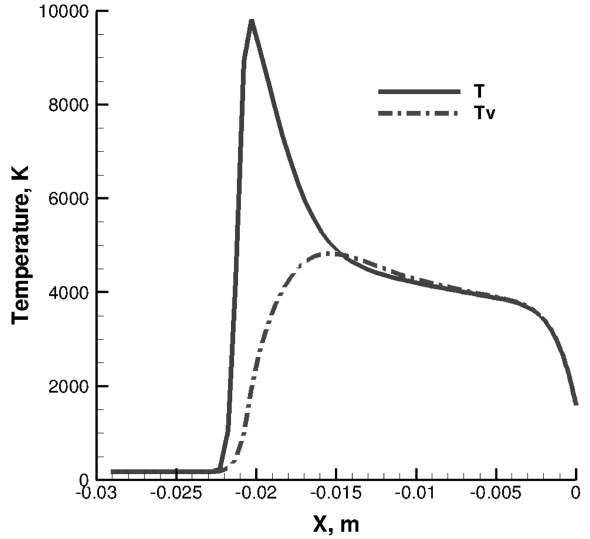

Fig. 6 Distributions of translational, rotational, and vibrational temperatures for the Mars atmosphere entry at 35 km along the stagnation line.

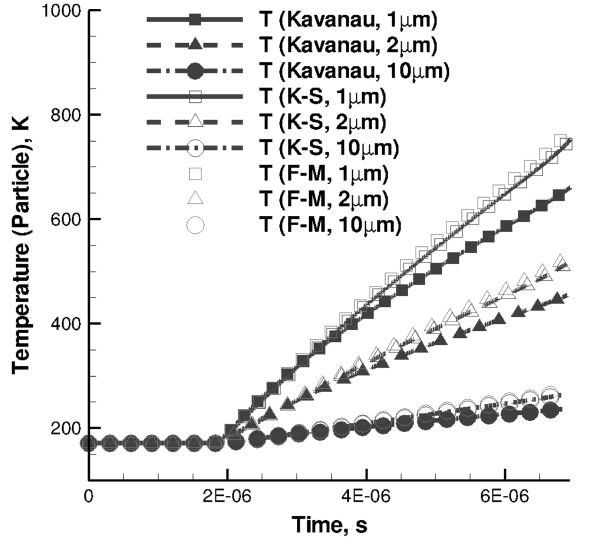

Fig. 8 Particle temperature change using the Mars atmosphere entry flowfield at 35 km with thermal decomposition.

viewpoint, our project focuses on dust samples greater than 1 μm size. For particles smaller than 1 μm, the aerogel capture and particle picking are significantly difficult. In addition, a 0.1 μm particle was simulated, and it was found that before reaching the spacecraft surface, the particle was evaporated due to the heating. Temperatures of 1-, 2-, and 10-μm-sized dust particles reach approximately 660, 450, and 250 K, respectively, using the modified Kavanau model when the particles impact the body. The difference between the K-S and F-M models is small, and using these models the maximum temperatures for 1-, 2-, and 10-μm-sized dust particles are roughly 740, 500, and 260 K, respectively. The temperature increase is the maximum in the stagnation region, and the temperature change is smaller when the particle trajectory goes farther away from the axisymmetric line as is shown in Fig. 9. Note that although the modified Kavanau model predicted the lowest particle temperature for trajectory 1, the difference is small among the three models for trajectory 2, and the modified Kavanau model predicted the highest particle temperature for trajectory 3.

To clarify the transition of the correlation among the three models from the stagnation to the downstream region, distributions of the particle Nusselt number Nu, Reynolds number Re_d, and Mach number M for the particle at three different locations as a function of time were investigated. The Mach number is based on the relative particle-flow velocity. In Figs. 10–12, comparisons of the Nusselt number, Reynolds number and Mach number are presented, respectively, for a 1 μm dust particle using the modified Kavanau model. It is shown that for particle paths starting further from the axis of symmetry, all the values (Nu, Re_d, and M) decrease, and as a given dust particle travels downstream toward the vehicle body, the values increase through the shock and near the body. By comparing the trajectories 1 and 3, the Mach number is decreased approximately from 3.5 to 2 inside the shock and the Reynolds number from 0.5 to 0.05. These changes also affect the change of the Nusselt number, and the value is approximately changed from 0.1 to 0.01. On the other hand, the drag coefficient C_D increases for particle paths starting further from the axis of symmetry. It is discussed in [13] that the K-S model is more sensitive to change of Re_d. Since the decrease of Re_d is more significant from the stagnation to the downstream region than the Mach number, the relation among the three models was also changed dramatically from the stagnation to downstream. The decrease of Nusselt number is more prominent in the K-S and F-M models from the stagnation to the downstream. The particle heating predicted by these two models is lower than the Kavanau model for trajectory 3 in contrast to the higher heating prediction in the stagnation region.

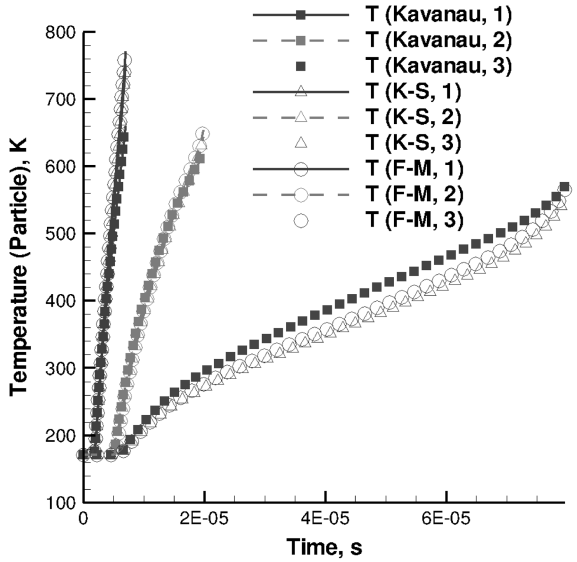

Fig. 9 Particle (1 μm) temperature change from three different initial locations using the Mars atmosphere entry flowfield at 35 km with thermal decomposition.

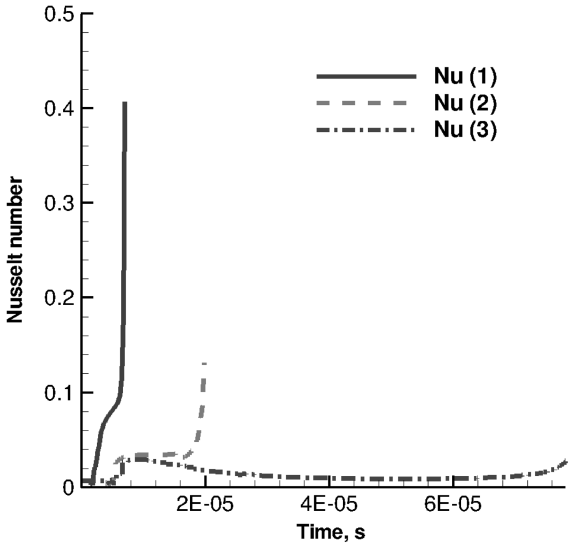

Fig. 10 Comparison of the Nusselt number change among the three different locations as a function of time at 35 km.

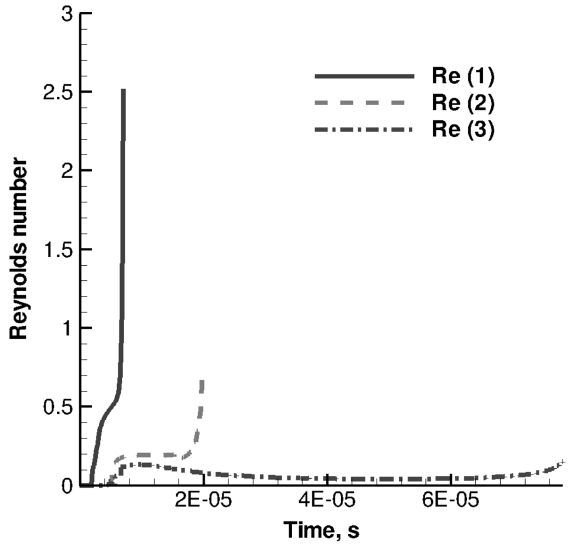

Fig. 11 Comparison of the Reynolds number change among the three different locations as a function of time at 35 km.

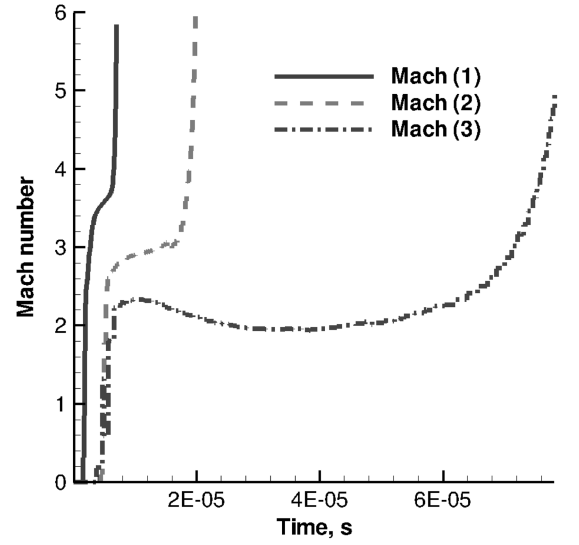

Fig. 12 Comparison of the Mach number change among the three different locations as a function of time at 35 km.

Table 5 Parameters in the flowfield at 35 km

Parameter	Case 1	Case 2	Case 3	Case 4
t, s	4.01×10^{-6}	6.01×10^{-6}	2.00×10^{-5}	6.00×10^{-5}
x, m	-1.20×10^{-2}	-4.14×10^{-3}	4.41×10^{-1}	5.82×10^{-1}
M	3.92	4.24	2.15	2.20
Re_d	0.55	0.72	8.52×10^{-2}	4.82×10^{-2}
ρ, kg/m^3	8.42×10^{-3}	9.83×10^{-3}	1.99×10^{-3}	1.11×10^{-3}
v_R, m/s	3839.5	3887.6	1495.24	1954.2
T_d, K	410	632	264	411
Kn ($L = 2$ μm)	3.1	2.69	13.26	23.7
C_D (macro)	2.32	2.32	2.87	2.77
C_D (DSMC)	2.34	2.34	2.85	2.85
C_h (Kavanau)	0.42	0.36	1.12	0.93
C_h (K-S)	0.43	0.39	0.86	0.77
C_h (F-M)	0.45	0.41	0.91	0.81
C_h (DSMC)	0.44	0.40	0.91	0.82
f_{Tad} (macro)	1.89	2.04	1.29	1.34
f_{Tad} (F-M)	2.35	2.57	1.44	1.523

Moreover, the dependency of the K-S and F-M models on the accommodation coefficient of the particle surface was investigated by comparing two cases of $\alpha = 1.0$ and 0.9 (see [67]). It was found that using a value of α of 0.9, the Nusselt number and temperature change rate are decreased, and the maximum temperature for a 1 μm dust particle is decreased by 40 K. Although the Kavanau model provides better agreement with the K-S model with $\alpha = 0.9$ for the flow condition of trajectory 1, the difference between the two models increases for trajectories 2 and 3. Even for the worst heating case predicted by the K-S and F-M models for $\alpha = 1.0$, these two models predict lower heating effects than the Kavanau model in the downstream region.

D. Investigations of Drag and Heat Transfer Coefficients at 35 Kilometers

To investigate the reliability of the macroscopic models, the drag and heat transfer coefficients were compared with the microscopic DSMC computations for the rarefied supersonic flow regime. Along the trajectories 1 and 3, two typical flow conditions (one is away from the body and lower density and another is near the body and higher density) were chosen, and 2-D axisymmetric DSMC calculations were performed. The selected coordinates and the flow conditions are listed in Table 5. The relative velocity, temperature, and total number density, as well as mole fractions of chemical species, are obtained for the DSMC calculations. For cases 1 and 2 on trajectory 1, the Knudsen number is lower than 5 and the Mach number is approximately 4 because of the low flow velocity in the stagnation region. For cases 3 and 4 on trajectory 3, the Knudsen number is higher than 10 and the M is approximately 2. By simulating flows around a sphere, C_D and C_h on the sphere were calculated for each flow condition. A dust radius of 1 μm for the sphere and the accommodation coefficient of 1.0 were used for the DSMC drag and heat transfer computations. The details of the vehicle DSMC calculations can be found in Sec. V.

To begin with, it can be seen in Table 5 that the drag coefficients obtained by the DSMC calculations agree appreciably well with the macroscopic results for all of the flow conditions. Second, the DSMC heat transfer coefficients agree well with the K-S and F-M models for cases 1 and 2. While the discrepancy between the Kavanau model and the DSMC is not large for case 1, it increases for case 2. These results agree with the particle temperature prediction for trajectory 1 shown in the previous subsection. For cases 3 and 4, because of the high Knudsen number, the C_h (DSMC) agrees with the F-M model the best, as expected. The K-S model predicts slightly lower C_h than the DSMC. The Kavanau model predicts considerably higher C_h than the other three results, and thus the Kavanau model predicted the highest particle temperature for trajectory 3. Furthermore, the effect of gas mixture in the DSMC calculations was found to be so small that the macroscopic calculations using the CO_2 properties are able to predict the particle heat transfer well. In summary, since the DSMC results are basically between the K-S and F-M models and these models predict similar particle temperatures, these two models are more reliable than the Kavanau model at 35 km.

E. Mars Flowfield at 45 Kilometers

In case that the Martian-dust distributions are influenced by dust storms, the feasibility of dust sample capture at 45 km was also investigated in this work. At 45 km altitude, the freestream number density is approximately 1/4 of the 35 km case, and the speed is 5 km/s, which is slightly higher than the 35 km (see Table 2). At this altitude, considering the lower density condition and the breakdown effect, 2-D axisymmetric DSMC computations which can compute three temperatures from the particle velocities and internal energies have been carried out for the Mars atmosphere entry flowfield, whereas the flow is still near continuum. For CO_2, the vibrational temperature is calculated as the average among the four vibrational modes. In Fig. 13, a contour plot of translational temperature for the Mars atmosphere entry at 45 km is shown, and the maximum temperature is approximately 17,000 K. In the figure, streamlines and particle trajectories are also compared from three different initial locations in the figure. The initial r coordinates are 0.01, 0.1, and 0.2 m for trajectories 4–6, respectively. It is seen that similar to the 35 km case, the trajectories of a dust particle are hardly influenced by the shock due to the heavy mass and do not follow the streamlines. Details of the Mars entry flowfield at 45 km along the stagnation line calculated by the DSMC method are shown in Figs. 14 and 15. The

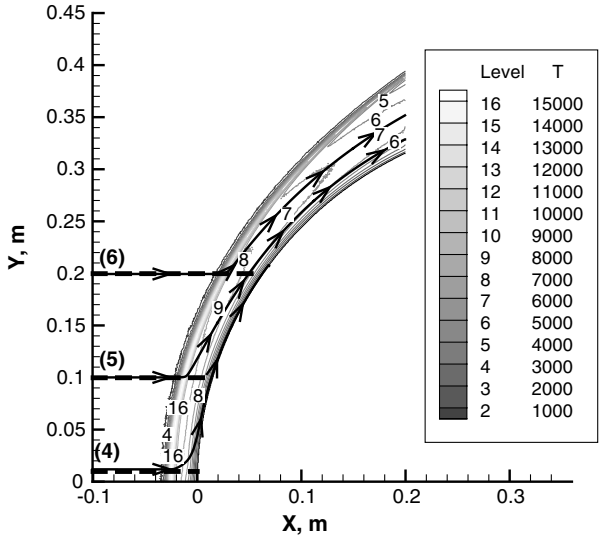

Fig. 13 Contour plot of temperature for the Mars atmosphere entry at 45 km and streamlines (solid line) and particle trajectories (dashed line).

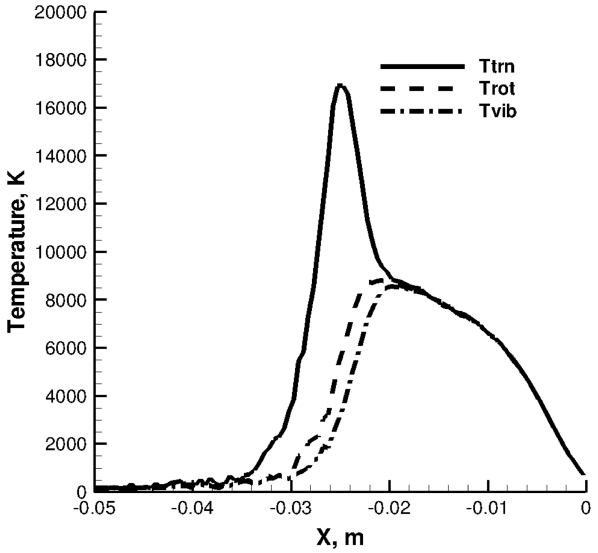

Fig. 14 Distributions of translational, rotational, and vibrational temperatures for the Mars atmosphere entry at 45 km along the stagnation line.

shock standoff distance at this altitude is approximately 2.5 cm, which is slightly larger than the 35 km case. The temperature overshoot phenomenon can be seen, and the maximum translational temperature is approximately 17,000 K. In the overshoot region, the rotational temperature is significantly lower than the translational temperature and slightly higher than the vibrational temperature. In other words, a two-temperature model, which is widely used in CFD, cannot predict the flowfield correctly in the overshoot region. The translational, rotational, and vibrational temperatures are approximately the same in the postshock region, and the temperature range is between 6000 and 8000 K. Dissociation processes of CO_2 are dominant inside the shock, and the number density increase of CO and O can be seen in Fig. 15. However, CO_2 is still the main species inside the shock despite the high dissociation processes, and thus CO_2 properties can be used for the macroscopic heat transfer calculations.

F. Dust Heat Transfer at 45 Kilometers

Dust-particle motion, heat transfer, and thermal decomposition were simulated in the Mars entry flowfield at 45 km. A rarefaction effect can be more important at this altitude than 35 km, and in the same way as the 35 km case, three heat transfer models were compared and discussed in this subsection. At this altitude, M based on the relative particle-flow velocity is between 3 and 4 inside the shock. C_D is approximately 2.3 inside the shock, and C_D is only slightly higher for a 1 μm particle than that for a 2 μm particle. In Fig. 16, the temperature increase in the dust particles along the stagnation line is compared among the modified Kavanau, K-S ($\alpha = 1.0$) and F-M ($\alpha = 1.0$) models for 1-, 2-, and 10-μm-sized dust particles. Inside the shock, the dust-particle temperature gradually increases, and the heating rate is higher for the smaller particle. Using the modified Kavanau model, temperatures of the 1-, 2-, and 10-μm-sized particles reach approximately 456, 328, and 192 K, respectively, when the particles impact the body. Using the K-S model with $\alpha = 1.0$, these temperatures are approximately 526, 372, and 208 K, and the difference between the K-S and F-M models is small. The difference between the Kavanau and K-S models is comparatively large, which is 70 K at most, and it is less than 10 K between the K-S and F-M models. These temperatures are lower than the 35 km case because of the lower density and heat transfer rate. In fact, compared with the case of 35 km, the maximum temperature for a 1 μm dust particle predicted by these models is decreased by roughly 200 K. Note that the particle simulations were also carried out in the downstream region, and similar features to the 35 km case were obtained. The K-S and F-M models predict a higher heating rate than the modified Kavanau model in the stagnation region, and as a dust particle moves downstream, the heating rate decreases, especially using the K-S and F-M models, and these two models predict lower particle temperature than the Kavanau model. This phenomenon is due to the lower sensitivity of the Kavanau model to the variance of Re_d.

Finally, the particle size decrease was also investigated, as well as the temperature increase at 35 and 45 km in Figs. 17 and 18, respectively. In the figures, changes of particle temperature and radius as a function of time for 1-, 2-, and 10-μm-sized particles are shown. At 35 km, because the temperature of dust particles is still lower than 740 K, the effect of thermal decomposition is negligibly small, and the radius ratio for 1–10 μm particles is uniform. Needless to say, at 45 km the maximum particle temperature is even lower, and thus the effect of thermal decomposition is negligible.

G. Investigations of Drag and Heat Transfer Coefficients at 45 Kilometers

Drag and heat transfer coefficients were compared with the microscopic DSMC results for the rarefied supersonic flow condition at 45 km, and the reliability of the three macroscopic models was investigated in the stagnation region. Along trajectory 4, three typical

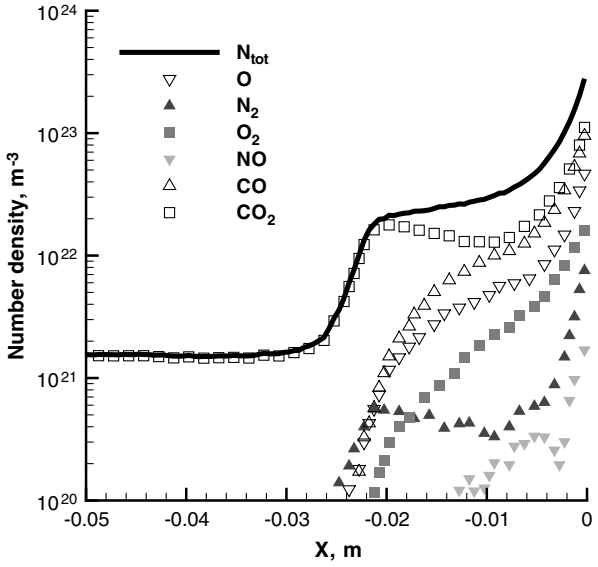

Fig. 15 Distributions of species number densities for the Mars atmosphere entry at 45 km along the stagnation line.

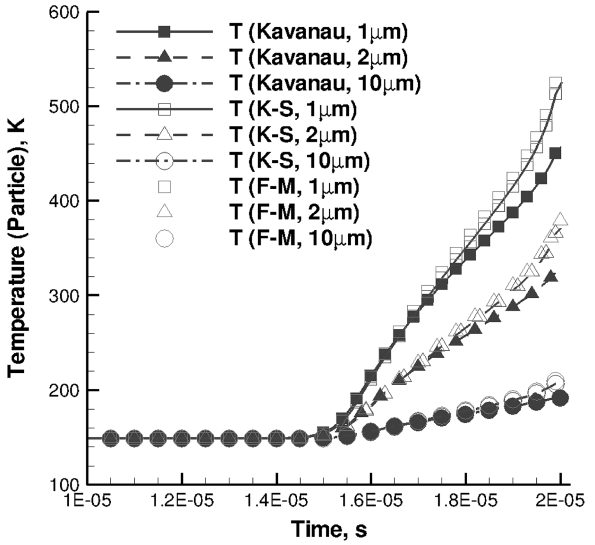

Fig. 16 Particle temperature change using the Mars atmosphere entry flowfield at 45 km with thermal decomposition.

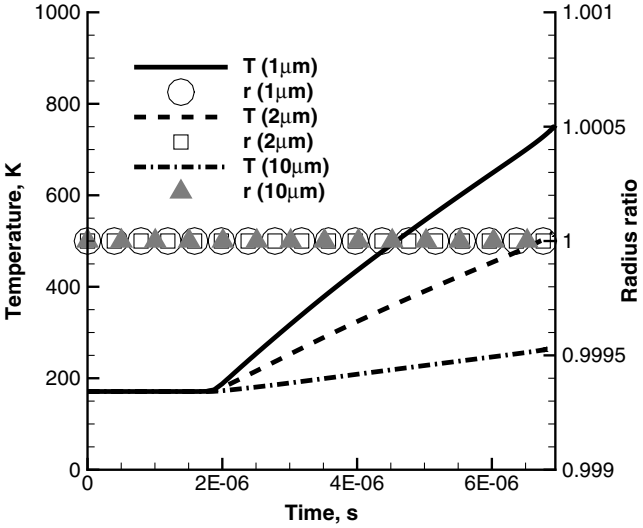

Fig. 17 Particle size decrease and temperature change using the Mars atmosphere entry flowfield at 35 km, due to thermal decomposition.

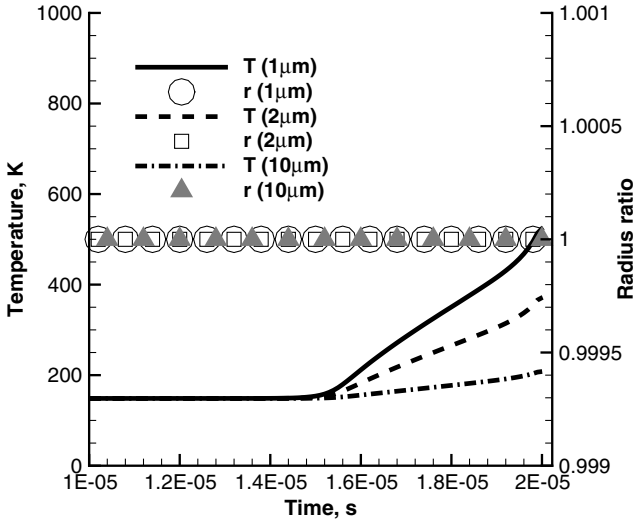

Fig. 18 Particle size decrease and temperature change using the Mars atmosphere entry flowfield at 45 km, due to thermal decomposition.

flow conditions were chosen and the selected coordinates and the flow conditions are listed in Table 6. The Kn, M, and Re_d significantly change while traveling through the shock along the trajectory, and thus the prediction of macroscopic models may be influenced by the flow condition transition. For case 1, the flow is in a supersonic, rarefied flow regime, where Kn is higher than 10, Re_d is lower than 0.1, and M is approximately 3.6. For case 2, Knudsen number is lower than 10, and M and Re_d are roughly 4.8 and 0.22, respectively. Case 3 is near the body, and Kn is considerably decreased, which is around 2.2. M and Re_d are approximately 8 and 1.7, respectively. For each condition, 2-D axisymmetric DSMC computations were carried out to simulate flows over a 1-μm-radius sphere to calculate the C_D and C_h. Details of the DSMC calculations are the same as the 35 km case.

Table 6 Parameters in the flowfield at 45 km

Parameter	Case 1	Case 2	Case 3
t, s	4.22×10^{-6}	6.02×10^{-6}	6.92×10^{-6}
x, m	-0.014	-0.005	-6.2×10^{-4}
M	3.58	4.75	8.06
Re_d	0.085	0.22	1.697
v_R, m/s	4768.3	4931.73	4926.98
Kn ($L = 2$ μm)	14.8	8.94	2.23
C_D (macro)	2.339	2.231	2.130
C_D (DSMC)	2.329	2.252	2.08
C_h (Kavanau)	0.50	0.34	0.173
C_h (K-S)	0.46	0.36	0.26
C_h (F-M)	0.51	0.39	0.27
C_h (DSMC)	0.50	0.38	0.26
f_{Tad} (macro)	1.73	2.29	6.42
f_{Tad} (F-M)	2.13	2.95	8.73

To start with, it is worth noting that good agreement on C_D is obtained between the macroscopic and DSMC results for all the cases. For case 1, with respect to C_h, good agreement was also found between the macroscopic and DSMC results, although the K-S model predicts a slightly lower value. For case 2, the C_h obtained by the DSMC agrees well with both of the K-S and F-M models. However, the Kavanau model predicts the lowest C_h. For case 3, similar feature to case 2 is observed. Nevertheless, the discrepancy between the Kavanau model and other results is increased. Overall, it was found that the DSMC results agree well with the K-S and F-M models, and the Kavanau model predicts the lower heat transfer rate. This corresponds to the particle temperature results in Fig. 16.

VII. Conclusions

The feasibility of capturing micron-sized Martian-dust particles for a Mars nonstop dust sample return project has been investigated in this work. The effect of a hot-temperature shock to micron-sized dust particles was estimated by simulating particle motion, heat transfer, and thermal decomposition. Moreover, the heat transfer rates were examined by comparing between three macroscopic models and microscopic calculations.

First, the floating-Martian-dust distributions were examined in the vertical direction and in the size, and it was found that there are a plenty of micron-sized dust particles between 30 and 40 km altitude in the average weather condition and for altitudes over 50 km in the dust-storm condition. All the models except one predicted similar distributions between 0.5 and 2 μm.

Second, CFD and DSMC flowfield calculations were performed for a spacecraft entry in the Martian atmosphere at 35 and 45 km altitudes. Although dissociation rates of CO_2 were high inside a shock, CO_2 was found to still be the major species in the postshock region at both altitudes. Temperature inside the shock was higher than 4000 K at both altitudes. Using the CO_2 properties, three heat transfer models (the modified Kavanau, K-S, and F-M models) were compared for the estimation of Martian-dust heating when dust particles travel through the hot-temperature shock. It was found that the discrepancy between K-S and F-M models is small for the dust sample conditions, and these two models predict higher particle temperature in the stagnation region than the modified Kavanau model. On the contrary, in the downstream region, the modified Kavanau model predicts higher particle temperature, since this model is less sensitive to the variance of Re_d compared with the other two models. The maximum dust-particle temperature at 35 km is observed in the stagnation region and is approximately 740 K using the K-S and F-M models for a 1 μm particle. At 45 km, the maximum T_d is only 530 K even in the stagnation region.

Finally, the reliability of macroscopic models in the rarefied, low Re_d, supersonic to hypersonic flow regime was discussed by being compared with the microscopic DSMC calculations. To sum up the major characteristics, the macroscopic drag coefficients are in good agreement with the DSMC results at both altitudes, and the K-S and F-M models agree better with the DSMC than the Kavanau model for C_h. In the downstream region, the K-S and F-M models predict lower heat transfer rates than the Kavanau model and the influence of a hot-temperature shock is lower, and it is therefore suitable to sample micron-sized dust particles in the downstream region. Furthermore, since thermal decomposition effects were found to be negligibly small, the micron-sized dust-particle sampling at these altitudes is possible and the dust constituents may not be destroyed while traveling through the shock. It should be noted that heating and sublimation of dust particles in a capturing medium, such as silica

aerogel, need to be considered for the overall evaluation, and in our future work, the effect of an aerogel impact and heating during a penetration of an aerogel is planned to be investigated by hypervelocity impact experiments.

References

[1] Yamamoto, T., and Tsuruda, K., "The PLANET-B Mission," *Earth, Planets and Space*, Vol. 50, No. 3, 1998, pp. 175–181.

[2] Kawaguchi, J., Uesugi, T., Fujiwara, A., and Matsuo, H., "The MUSES-C, World's First Sample and Return Mission from near Earth Asteroid: NEREUS," *Acta Astronautica*, Vol. 39, Nos. 1–4, 1996, pp. 15–23. doi:10.1016/S0094-5765(96)00118-X

[3] Sawai, S., "Development of Sample Collectors for the Sample and Return from Nereus in 2002," IAF Paper 95-U.4.04, 1995.

[4] Kawaguchi, J., Fujiwara, A., and Uesugi, T., "Hayabusa–Its Technology and Science Accomplishment Summary and Hayabusa-2," *Acta Astronautica*, Vol. 62, Nos. 10–11, 2008, pp. 639–647. doi:10.1016/j.actaastro.2008.01.028

[5] Fujita, K., Tachibana, S., Sugita, S., Miyamoto, H., Mikouchi, T., Suzuki, T., et al., "Preliminary Study of Nonstop Mars Sample Return System Using Aerocapture Technologies," AIAA Atmospheric Flight Mechanics Conference, AIAA Paper 2009-5614, Chicago, Aug. 2009.

[6] Fujita, K., Kubota, T., Ogawa, J., Yano, M., Suzuki, T., Takayanagi, H., et al. "Assessment of Aeroassist Orbital Maneuver Technologies for Next Mars Exploration," *27th International Symposium on Space Technology and Science*, ISTS Paper 2009-k-25, Tsukuba, Ibaraki, Japan, July 2009.

[7] Fujita, K., Tachibana, S., Miyamoto, H., Mikouchi, T., Suzuki, T., Takayanagi, H., et al. "Preliminary Study of Nonstop Mars Sample Return System Using Aerocapture Technologies," *27th International Symposium on Space Technology and Science*, ISTS Paper 2009-k-26, Tsukuba, Ibaraki, Japan, July 2009.

[8] Leshin, L. A., Yen, A., Clark, B., Forney, L., Gamber, T., Jones, S., et al. "Sample Collection for Investigation of Mars (SCIM): Study of an Early Mars Sample Return Mission Through the Mars Scout Program," *Meteoritics & Planetary Science*, Vol. 36, No. 9, Sept. 2001, p. A113.

[9] Takayanagi, H., Suzuki, T., and Fujita, K., "Feasibility Assessment of Nonstop Mars Sample Return System," 48th AIAA Aerospace Sciences Meeting and Exhibit, AIAA Paper 2010-0627, Orlando, FL, Jan. 2010.

[10] Leshin, L., "Sample Collection for Investigation of Mars (SCIM): An Early Mars Sample Return Mission Through the Mars Scout Program," *34th COSPAR Scientific Assembly*, Vol. 34, 2002.

[11] Jurewicz, A. J. G., Forney, L., Bomba, J., Vicker, D., Jones, S. M., Yen, A., et al., "Investigating the Use of Aerogel Collectors for the SCIM Martian-Dust Sample Return," *Lunar and Planetary Institute Science Conference Abstracts*, edited by S. Mackwell, and E. Stansbery, Vol. 34, March 2003, pp. 1703–+.

[12] Torobin, L. E., and Gauvin, W. H., "Fundamental Aspects of Solids-Gas Flow," *Canadian Journal of Chemical Engineering*, Vol. 37, 1959, pp. 129–141. doi:10.1002/cjce.5450370401

[13] Nelson, H. F., and Fields, J. C., "Particle Drag Coefficient in Solid Rocket Plumes," *Journal of Thermophysics and Heat Transfer*, Vol. 9, No. 3, 1995, pp. 567–569. doi:10.2514/3.707

[14] Nelson, H. F., and Fields, J. C., "Heat Transfer in Two Phase Solid Rocket Plumes," 30th AIAA Thermophysics Conference, AIAA Paper 1995-2131, San Diego, CA, June 1995.

[15] Walsh, M. J., "Drag Coefficient Equations for Small Particles in High Speed Flows," *AIAA Journal*, Vol. 13, No. 11, 1975, pp. 1526–1528. doi:10.2514/3.7026

[16] Henderson, C. B., "Drag Coefficients of Spheres in Continuum and Rarefied Flows," *AIAA Journal*, Vol. 14, No. 6, 1976, pp. 707–708. doi:10.2514/3.61409

[17] Melosh, H. J., and Goldin, T. J., "Heat and Drag Coefficients for Reentry of Impact Ejecta," *Lunar and Planetary Institute Science Conference Abstracts*, Vol. 39, March 2008, pp. 2457–2458.

[18] Kavanau, L. L., "Heat Transfer from Spheres to a Rarefied Gas in Subsonic Flow," *Transactions of the ASME. Journal of Tribology*, Vol. 77, No. 5, 1955, pp. 617–623.

[19] Koshmarov, Y. A., and Svirshevskii, S. B., "Heat Transfer from a Sphere in the Intermediate Dynamics Region of a Rarefied Gas," *Fluid Dynamics*, Vol. 7, No. 2, 1972, pp. 343–346. doi:10.1007/BF01186485

[20] Drake, R. M., and Backer, G. H., "Heat Transfer From Spheres to a Rarefied Gas in Supersonic Flow," *Transactions of the American Society of Mechanical Engineers*, Vol. 74, No. 7, Oct. 1952, pp. 1241–1250.

[21] Toon, O. B., Pollack, J. B., and Sagan, C., "Physical Properties of the Particles Composing the Martian Dust Storm of 1971–1972," *Icarus*, Vol. 30, 1977, pp. 663–696. doi:10.1016/0019-1035(77)90088-4

[22] Clancy, R. T., Lee, S. W., Gladstone, G. R., McMillan, W. W., and Rousch, T., "A New Model for Mars Atmosphere Dust Based upon Analysis of Ultraviolet Through Infrared Observations," *Journal of Geophysical Research*, Vol. 100, No. E3, 1995, pp. 5251–5263. doi:10.1029/94JE01885

[23] Ozawa, T., and Fujita, K., "Investigation of the Martian-Dust Capture for Mars Sample Return Mission," *53rd SSTC Conference*, SSTC Paper 2009-1g16, Kyoto, Japan, Sept. 2009.

[24] Yonemura, S., Tanaka, T., and Tsuji, Y., "Cluster Formation in Dispersed Gas-Solid Flow," *Proceedings of The 2nd International Conference on Multiphase Flow*, Kyoto, Japan, April 1995, pp. PT4-25–PT4-30.

[25] Tanaka, T., Yonemura, S., Kiribayashi, K., and Tsuji, Y., "Cluster Formation and Particle-Induced Instability in Gas-Solid Flows Predicted by the DSMC Method," *JSME International Journal, Series B (Fluids and Thermal Engineering)*, Vol. 39, No. 2, 1996, pp. 239–245.

[26] Kim, I., Elghobashi, S., and Sirignano, W. A., "On the Equation for Spherical-Particle Motion: Effect of Reynolds and Acceleration Numbers," *Journal of Fluid Mechanics*, Vol. 367, 1998, pp. 221–253. doi:10.1017/S0022112098001657

[27] Berlemont, A., Desjonqueres, P., and Gouesbet, G., "Particle Lagrangian Simulation in Turbulent Flows," *International Journal of Multiphase Flow*, Vol. 16, No. 1, 1990, pp. 19–34. doi:10.1016/0301-9322(90)90034-G

[28] Crowe, C. T., "Drag Coefficient of Particles in a Rocket Nozzle," *AIAA Journal*, Vol. 5, No. 5, 1967, pp. 1021–1022. doi:10.2514/3.4119

[29] Suzuki, T., Furudate, M., and Sawada, K., "Unified Calculation of Hypersonic Flowfield for a Reentry Vehicle," *Journal of Thermophysics and Heat Transfer*, Vol. 16, No. 1, 2002, pp. 94–100. doi:10.2514/2.6656

[30] Fujita, K., Sumi, T., Yamada, T., and Ishii, N., "Heating Environments of a Venus Entry Capsule in a Trail Balloon Mission," *Journal of Thermophysics and Heat Transfer*, Vol. 20, No. 3, 2006, pp. 507–516. doi:10.2514/1.18187

[31] Bird, G. A., *Molecular Gas Dynamics and the Direct Simulation of Gas Flows*, Clarendon, Oxford, 1994.

[32] Vesovic, V., and Wakeham, W. A., "The Transport Properties of Carbon Dioxide," *Journal of Physical and Chemical Reference Data*, Vol. 19, No. 3, 1990, pp. 763–808. doi:10.1063/1.555875

[33] Zeller, R. C., and Pohl, R. O., "Thermal Conductivity and Specific Heat of Noncrystalline Solids," *Physical Review B*, Vol. 4, No. 6, 1971, pp. 2029–2041. doi:10.1103/PhysRevB.4.2029

[34] Chase, M. W., Jr., *NIST-JANAF Thermochemical Tables, Fourth Edition*, Journal of Physical and Chemical Reference Data, Monograph, No. 9, American Chemical Society, Woodbury, NY, 1998.

[35] Carlson, D. J., and Hoglund, R. F., "Particle Drag and Heat Transfer in Rocket Nozzles," *AIAA Journal*, Vol. 2, No. 11, 1964, pp. 1980–1984. doi:10.2514/3.2714

[36] Sauer, F. M., "Convective Heat Transfer from Spheres in a Free-Molecule Flow," *Journal of the Aeronautical Sciences*, Vol. 18, No. 5, 1951, pp. 353–354.

[37] Oppenheim, A. K., "Generalized Theory of Convective Heat Transfer in a Free-Molecule Flow," *Journal of the Aeronautical Sciences*, Vol. 20, No. 1, Jan. 1953, pp. 49–58.

[38] Bird, B. R., Stewart, W. E., and Lightfoot, E. N., *Transport Phenomena*, Wiley, New York, 2002.

[39] Ferguson, F. T., and Nuth, J. A. I., "Vapor Pressure of Silicon Monoxide," *Journal of Chemical and Engineering Data*, Vol. 53, No. 12, 2008, pp. 2824–2832. doi:10.1021/je800560b

[40] Fujita, K., Suzuki, T., and Matsuyama, S., "Development of JAXA Optimized Nonequilibrium Aerothermodynamic Analysis Code," *The Japan Society of Fluid Mechanics Conference*, Toyo University, Tokyo, Sept. 2009.

[41] Park, C., and Ahn, H.-K., "Stagnation-Point Heat Transfer Rates for Pioneer-Venus Probes," *Journal of Thermophysics and Heat Transfer*, Vol. 13, No. 1, 1999, pp. 33–41. doi:10.2514/2.6426

[42] Park, C., Howe, J. T., Jaffe, R. L., and Candler, G. V., "Review of Chemical-Kinetic Problems of Future NASA Mission, II: Mars

Entries," *Journal of Thermophysics and Heat Transfer*, Vol. 8, No. 1, 1994, pp. 9–23.
doi:10.2514/3.496

[43] Park, C., Jaffe, R. L., and Partridge, H., "Chemical-Kinetic Parameters of Hyperbolic Earth Entry," *Journal of Thermophysics and Heat Transfer*, Vol. 15, No. 1, 2001, pp. 76–90.
doi:10.2514/2.6582

[44] Rock, S. G., Candler, G. V., and Hornung, H. G., "Analysis of Thermo-chemical Nonequilibrium Models for Carbon Dioxide Flows," *AIAA Journal*, Vol. 31, No. 12, 1993, pp. 2255–2262.
doi:10.2514/3.11923

[45] Fujita, K., and Abe, T., "SPRADIAN, Structured Package for Radiation Analysis: Theory and Application," Institute of Space and Astronautical Science report 669, Kanagawa, Japan, Sept. 1997.

[46] Capitelli, M., Gorse, C., Longo, S., and Giordano, D., "Collision Integrals of High-Temperature Air Species," *Journal of Thermophysics and Heat Transfer*, Vol. 14, No. 2, 2000, pp. 259–268.
doi:10.2514/2.6517

[47] Levin, E., and Wright, M. J., "Collision Integrals for Ion-Neutral Interactions of Nitrogen and Oxygen," *Journal of Thermophysics and Heat Transfer*, Vol. 18, No. 1, 2004, pp. 143–147.
doi:10.2514/1.2552

[48] Wada, Y., and Liou, M. S., "A Flux Splitting Scheme with High-Resolution and Robustness for Discontinuities," AIAA Paper 1994-0083, Jan. 1994.

[49] van Leer, B., "Towards the Ultimate Conservative Difference Scheme. V. A Second-Order Sequel to Godunov's Method," *Journal of Computational Physics*, Vol. 32, No. 1, 1979, pp. 101–136.
doi:10.1016/0021-9991(79)90145-1

[50] Eberhardt, S., and Imlay, S., "Diagonal Implicit Scheme for Computing Flows with Finite Rate Chemistry," *Journal of Thermophysics and Heat Transfer*, Vol. 6, No. 2, 1992, pp. 208–216.
doi:10.2514/3.347

[51] Bird, G. A., "Monte-Carlo Simulation in an Engineering Context," *Rarefied Gas Dynamics*, edited by S. Fisher, Vol. 74, AIAA, New York, 1981, pp. 239–255.

[52] Borgnakke, C., and Larsen, P. S., "Statistical Collision Model for Monte Carlo Simulation of Polyatomic Gas Mixture," *Journal of Computational Physics*, Vol. 18, No. 4, 1975, pp. 405–420.
doi:10.1016/0021-9991(75)90094-7

[53] Millikan, R. C., and White, D. R., "Systematics of Vibrational Relaxation," *Journal of Chemical Physics*, Vol. 39, No. 12, 1963, pp. 3209–3213.
doi:10.1063/1.1734182

[54] Parker, J. G., "Rotational and Vibrational Relaxation in Diatomic Gases," *Physics of Fluids*, Vol. 2, No. 449, 1959.
doi:10.1063/1.1724417

[55] Hash, D. B., and Hassan, H. A., "Monte Carlo Simulation of Entry in the Martian Atmosphere," *Journal of Thermophysics and Heat Transfer*, Vol. 7, No. 2, 1993, pp. 228–232.
doi:10.2514/3.411

[56] Murphy, J. R., Haberle, R. M., Toon, O. B., and Pollack, J. B., "Martian Global Dust Storms: Zonally Symmetric Numerical Simulations Including Size-Dependent Particle Transport," *Journal of Geophysical Research*, Vol. 98, No. E2, Feb. 1993, pp. 3197–3220.
doi:10.1029/92JE02945

[57] Pollack, J. B., Ockert-Bell, M. E., and Shepard, M. K., "Viking Lander Image Analysis of Martian Atmospheric Dust," *Journal of Geophysical Research*, Vol. 100, No. E3, March 1995, pp. 5235–5250.
doi:10.1029/94JE02640

[58] Odaka, M., "Martian Dust and Dust Storms," *Earozoru Kenkyu*, Vol. 22, No. 2, 2007, pp. 87–94 (in Japanese).

[59] Conrath, B. J., "Thermal Structure of the Martian Atmosphere during the Dissipation of the Dust Storm of 1971," *Icarus*, Vol. 24, 1975, pp. 36–46.
doi:10.1016/0019-1035(75)90156-6

[60] Pollack, J. B., Colburn, D., Kahn, R., Hunter, J., Camp, W. V., Carlston, C. E., and Wolf, M. R., "Properties of Aerosols in the Martian Atmosphere, as Inferred from Viking Lander Imaging Data," *Journal of Geophysical Research*, Vol. 82, No. 28, Sept. 1977, pp. 4479–4496.
doi:10.1029/JS082i028p04479

[61] Dlugach, Z. M., and Morozhenko, A. V., "Parameters of Dust Particles in the Martian Atmosphere," *Solar System Research*, Vol. 35, No. 6, 2001, pp. 421–430.
doi:10.1023/A:1013091027203

[62] Korablev, O. I., Krasnopolsky, V. A., and Rodin, A. V., "Vertical Structure of Martian Dust Measured by Solar Infrared Occultations from Phobos Spacecraft," *Icarus*, Vol. 102, 1993, pp. 76–87.
doi:10.1006/icar.1993.1033

[63] Chassefiere, E., Blamont, J. E., Krasnopolsky, V. A., Korablev, O. I., Atreya, S. K., and West, R. A., "Vertical Structure and Size Distributions of Martian Aerosols from Solar Occultation Measurements," *Icarus*, Vol. 97, 1992, pp. 46–69.
doi:10.1016/0019-1035(92)90056-D

[64] Markiewicz, W. J., Sablotny, R. M., Keller, H. U., Thomas, N., Titov, D., and Smith, P. H., "Optical Properties of the Martian Aerosols as Derived from Imager for Mars Pathfinder Midday Sky Brightness Data," *Journal of Geophysical Research*, Vol. 104, No. E4, April 1999, pp. 9009–9017.
doi:10.1029/1998JE900033

[65] Tomasko, M. G., Doose, L. R., Lemmon, M., Smith, P. H., and Wegryn, E., "Properties of Dust in the Martian Atmosphere from the Imager on Mars Pathfinder," *Journal of Geophysical Research*, Vol. 104, No. E4, April 1999, pp. 8987–9007.
doi:10.1029/1998JE900016

[66] Justh, H. L., and Justus, C. G., "Mars Global Reference Atmospheric Model (Mars-GRAM 2005) Applications for Mars Science Laboratory Mission Site Selection Processes," *7th International Conference on Mars*, 2005.

[67] Ozawa, T., Suzuki, T., Takayanagi, H., and Fujita, K., "Modeling of Martian Dust Collection for Non-stop Mars Sample Return Mission," 48th AIAA Aerospace Sciences Meeting, AIAA Paper 2010-0886, Orlando, FL, Jan. 2010.